Anomalous Diffusion of Water in Biological Tissues

M. Köpf,* C. Corinth,* O. Haferkamp,* and T. F. Nonnenmacher‡
*Department of Pathology and ‡Department of Mathematical Physics, University of Ulm, 89061 Ulm, Germany

ABSTRACT This article deals with the characterization of biological tissues and their pathological alterations. For this purpose, diffusion is measured by NMR in the fringe field of a large superconductor with a field gradient of 50 T/m, which is rather homogenous and stable. It is due to the unprecedented properties of the gradient that we are able not only to determine the usual diffusion coefficient, but also to observe the pronounced Non-Debye feature of the relaxation function due to cellular structure. The dynamics of the probability density follow a stretched exponential or Kohlrausch-Williams-Watts function. In the long time limit the Fourier transform of the probability density follows a long-tail Lévy function, whose asymptotic is related to the fractal dimension of the underlying cellular structure. Some of the properties of Lévy walk statistics are discussed and its potential importance in understanding certain biophysical phenomena like diffusion processes in biological tissues are pointed out. We present and discuss for the first time NMR data giving evidence for Lévy processes that capture the essential features of the observed power law (scaling) dynamics of water diffusion in fresh tissue specimens: carcinomas, fibrous mastopathies, adipose and liver tissues.

INTRODUCTION

Increased clinical interest in pathological tissue characterization by the method of NMR (Cheng, 1993; Hazlewood et al., 1991; Ishida et al., 1995; Le Bihan et al., 1986; Norris et al., 1994) has lead to the relatively new discipline of synthetic image calculation with the result that diffusion imaging might lead to comparable or even better contrasts than the well-known and widely used NMR parameters, T_1 and T_2 (Cheng, 1993). The major difference between the commonly used methods and the present method is that the former contain spatially resolved information about the physiological state of tissues. The investigated areas are generally large, ranging from a few centimeters to whole body pictures. The associated gradients are small and can be obtained by switching gradient coils, as required for in vivo investigations. Depending on the kind of research topic, method, and instrumental equipment, deviation from the normal or Debye behavior are of minor importance (Le Bihan, 1986) or are handeled by phenomenological modelling (Cheng, 1993). Complementary to these methods, the length scales covered by the present method are all together in the subcellular region (<100 μ). Instead of getting a spatial picture we focus on the dynamic properties of water and fat within a selected thin sheet. Depending upon the type of relaxation function, we get information about the distribution of length scales of fluctuations within this sheet. The influence of cellular structure leads to deviations from the Debye behavior and is central to the method. Until now mainly pilot investigations of well-selected model systems with a specific structure have been carried out at comparatively low gradients (Tanner and Steijskal, 1968; Callaghan, 1991) to verify the NMR characteristics of diffusion at least in specific cases. The possibility of using the extremely strong and stable gradient field of a large superconductor was recognized only recently (Kimmich et al., 1991); as of now only a few investigations (Kimmich et al., 1991, 1994a, 1994b; Fujara et al., 1994) are available. Of special interest in these investigations are the characteristic deviations from the normal diffusional behavior, which establish clearly in the long-time asymptotics with signal amplitudes of only a small percentage of the initial amplitude. Thus rather accurate and time-extensive measurements are necessary to get acceptable signal/noise ratios, even for these model systems. The deviations are characteristic of the kind of hindrance of free diffusion by barriers, compartmentation, tubes, and bonds involving specific length and time scales. The field gradient is connected to a "wave vector" or spatial encoding of nuclear spins. The available field gradients in the usual pulsed-gradient, stimulated-echo method are rather small. The corresponding length scale largely exceeds cellular dimensions. Therefore the influence of cellular structure is well treated by approximate solutions of the diffusion equation with boundary conditions. Complementary to these methods, the field gradient in the supercon fringe field method (Kimmich et al., 1991, 1994a) exceeds the field gradient of the pulsed-gradient, stimulated-echo method by orders of magnitude, thus leading to length scales well within subcellular regions. Therefore, quite extended models of data description were expected to apply in our study of enhanced spatial resolution (because of the large field gradient), which ranges from approximately 15 to 1 μm. "Resolution" in this context gives a rough estimate of the minimum rms-distance a molecule must move to sense the spatial encoding by the gradient. In the range of available time scales and wave vectors, all presented measurements of biological tissue are dynamic as a sharp boundary is not reached by an appreciable fraction bulk water. Instead of such a precise length scale, a self similar series of length

Received for publication 5 April 1995 and in final form 15 March 1996.
Address reprint requests to Dr. Manfred Köpf, Department of Pathology, University of Ulm, Albert Einstein Allee 11, 89069 Ulm, Germany. Tel: 49-731502-2990; Fax: 49-731502-3003.

0006-3495/96/06/2950/09 $2.00

scales is observed on a structure with fractal dimension. We show that some of these features can be explained within the context of Lévy statistics (Nonnenmacher, 1994; Nonnenmacher and Nonnenmacher, 1989; Glöckle and Nonnenmacher, 1993; Metzler et al., 1994; Zumofen et al., 1989; Montroll and Bendler, 1984; West and Shlesinger, 1989; West and Deering, 1994) that have recently been applied to physiology (West and Deering, 1994), to ion channel gating kinetics (Nonnenmacher and Nonnenmacher, 1989; Nonnenmacher, 1994; West and Deering, 1994), and to self similar protein dynamics (Glöckle and Nonnenmacher, 1995).

The fractal scaling of lengths determines the form of the probability density over the range of the evolutionary time scale, accessible to the NMR measurement, i.e., 2–200 ms. According to the stimulated echo method, we are able to observe either the dynamic evolution of the probability density in time or its spatial form at fixed time. The former is best described by a Kohlrausch-Williams-Watts (KWW) function, the latter by a power law for long evolutionary times. The kind of observed relaxation function is quite different for short, intermediate, and long time scales (T) and furthermore dependent on cellular structure.

The observed relaxation functions are either

$$E = \exp(-Db) \qquad \text{(Debye)} \qquad (1)$$

$$E = \exp - (Db)^{\alpha} \qquad \text{(KWW)} \qquad (2)$$

$$E \sim (q^2)^{-\mu} \qquad \text{(power law)} \qquad (3)$$

The forms (Eqs. 2 and 3) well describe the asymptotic decays for glandular and fibrous tissues. In contrast fatty tissues were described best by the Debye form (Eq. 1).

This means an absence of smaller cellular details and is generally observed in fatty tissues, whose cells show this feature. In contrast cancerous tissue is highly structured because of enlarged number or mitoses, irregular cell form, and enhanced nucleus/plasma relation. Thus water molecules in the cancer cell experience a hierarchy of structure that extends to much smaller scales than in well differentiated cells. Sometimes these features are shared with glandular or fibrous tissues and make a distinction difficult.

The quantity b in Eqs. 1 and 2 involves the time scale of measurement (T), the experimentally given evolutionary time, and a length scale, given by a wave vector q with the interrelation

$$b = 4\pi^2 q^2 T \qquad (4)$$

and D is the usual diffusion coefficient. The Debye behavior (Eq. 1) is in general only valid for pure fluids or fatty tissue because of the low degree of compartmentation. For glandular or fibrous tissue, Eq. 1 holds only for short times (T) due to the contribution of free water (Drost-Hansen and Clegg, 1976; Hazlewood et al.., 1974). For longer T, a superposition of Eqs. 1 and 2 is necessary for the description of the dynamics of the diffusion process. The Fourier description of probability density at long, fixed T is most suitable described by Eq. 3. The exponent μ in Eq. 3 involves the fractal dimension of the underlying geometry.

The often appearing quantity Db can be read as a measure of ensemble-averaged mean square displacement, hypothetically measured along the contour of microscopic structure (here in the cellular length scale), which is by no means identical to the actually measured displacement (by the wave vector "q") in Euclidean space. Considering the above-mentioned limited time scale accessible to NMR, the following peculiarities are obvious: For short evolutionary times T, the diffusing water molecules do not have enough time to sense appreciable features of the local cellular structure, so that the relaxation function is nearly of the Debye form (Eq. 1). At increased times, large mean square displacements are always a superposition of smaller ones and it is exactly the distribution function of these that is measured. In the absence of structure on small length scales, displacements on these scales are no more accessible at large times. The essential difference between the models (Eqs. 2 and 3) is expressed in different large q-asymptotic as a curved or straight line, respectively. Details are given in the appendix.

MATERIALS

Fresh tissue specimens were obtained routinely a few minutes after excision from the operating rooms and immediately adjusted to the NMR probe; probe head and sample were held at a constant temperature of 4°C to minimize degradation processes of the tissues (autolysis). Under these widely constant conditions 12 carcinomas, 15 fibrous mastopathies, and 5 fatty tissues were investigated. Among the carcinomas there were 2 specimens without fat. To test the method's sensitivity to the influence of specified tissue structure (glandular, fibrous, and solid) different kinds of tissue such as thyroid gland (3), muscle (4), and liver (2) were examined (number of samples in brackets). The NMR investigation lasted between a few hours and one day; routinely additional T_1-measurements were performed (within 10 min) up to five times per sample (beginning, middle, and end of the main measurements) to have a control over eventually occurring alterations of the sample that were not observed. After the NMR investigation the specimens were put in 4% formalin buffer and conserved for histology.

METHODS

Diffusion was measured by the method of the stimulated echo in the fringe field of the 9.4 T/8.9 cm bore magnet of a Bruker MSL 400 spectrometer (Karlsruhe, Germany). At 26-cm axial distance from magnet center the flux density is B_0 = 3.9 T, corresponding to 162-MHz proton Larmor frequency. A ^{31}P high power probehead of the Bruker MSL 400 was used. It provided the appropriate tuning range for protons in this application. Moreover at this axial distance the field gradient reached its maximum of 50 T/m. This reading was nearly constant over 2 cm and radially flat within 100 KHz over half the bore diameter. The 90° pulse length was 4 μs. In the presence of the strong field gradient, even such short RF pulses are soft; thus, only 100-μm-thick slices are activated and recorded. With each sample two series of measurements were performed: First the wave vector was held fixed, choosing τ_1 = 40, 70, and 100 μs, and varying the long evolution interval τ_2 from 300 μs to 1 s. This first series gives information about the dynamics of the diffusion process, i.e., the evolution of the rms-displacement, which follows a KWW function (Eq. 2). In the second series, τ_2 was held fixed at logarithmically equidistant intervals, ranging from 2 to 320 ms and τ_1 was varied from 40 to 600 μs. In this series the dynamics of the diffusion process are effectively screened out, thus yield-

ing a Fourier description of the probability density at fixed time (Eq. 3). At longer τ_2 the amplitudes are no longer coincident even at small q vectors, but diminish significantly because of an efflux of activated triglycerides from the thin slice of tissue, not essentially larger than the diameter of the fat cell. The evolution in time is described by a single Debye function with a significantly smaller diffusion coefficient due to the triglycerides as the dominating components. This effect is most pronounced on the right graph of Fig. 2, below.

Data evaluation

According to our setup we have two principal methods of measurement. First, keeping the preparation interval, τ_1, or the wave vector small but fixed and second, stepping the longer evolution interval, τ_2, we get information about the dynamics. For glandular or fibrous tissue the relaxation process is described by a superposition of a Debye function and a process of anomalous diffusion:

$$E = C_1 \exp[-Db] + C_2 \exp - (Db)^{\alpha} \qquad (5)$$

The fractions C_1 and C_2 represent the relative contributions of free and bound cellular water (Drost-Hansen and Clegg, 1976; Hazlewood et al., 1974). The presence of the first term is indicated by more-or-less pronounced dips or inflection points in the relaxation function under τ_2-variation. Further it is physiologically motivated by the fact, that ~90% of cellular water is free and only 10% is bound to macromolecules; the two compartments do not exchange to an appreciable amount in the time scale of measurement τ_2. The bound contribution presents a microscopic heterogeneity that is not averaged out on the time scale of measurement, i.e., within milliseconds. Multi-exponential behavior of relaxation that has been reported (Hazlewood et al., 1974; McSweeney et al., 1984; Bottomley et al., 1984), and the reduction in the diffusion coefficient are not explained by the fast exchange model, which holds only for simple solutions such as protein solutions with physiological concentrations (Taylor et al., 1988). The effect of compartmentation however leads to the presence of isolated submagnetizations. In tissues with appreciable fatty content, and hence macroscopic heterogeneity (Bottomley et al., 1984), the second term in Eq. 5 is overshadowed by the relaxation function of fat. The fatty contribution follows a Debye function with a significantly different diffusion coefficient than triglycerides:

$$E = C_1' \exp[-D_1 b] + C_2' \exp[-D_2 b). \qquad (6)$$

In Eq. 6, D_1 and D_2 represent the diffusion coefficient of water in fibroglandular and triglycerides in fatty parts with contributions $C1'$ and $C2'$.

A distinction between these cases is sometimes difficult but necessary in the presence of large error estimates if one tries the wrong function.

With the second method—keeping τ_2 fixed and stepping the wave vector—(according to Callaghan (1991)) we formally get the square of a Fourier description of the spatial probability density at time τ_2. The form (Eq. 3) is mostly evident for long τ_2-values when the molecules begin to sense structure. The asymptotic (Eq. 3) is often only evident at the longest accessible τ_2-values (100–200 ms). In between, sometimes tremendous deviations from Eq. 3 occur, but the described trend of the asymptotic is persistent and was used for determination of μ and was performed by visual inspection of the relaxation function at longest τ_2.

RESULTS

In a first section we show characteristic relaxation functions for the investigated specimen and describe their features. All relaxation functions are given in a double logarithmic plot. A Debye function (Eq. 1) or KWW function (Eq. 2) appear curved, whereas a power law (Eq. 3) gives a straight line in this representation. This representation was chosen to cover the very large range of echo amplitudes (4 decades) and b-values (up to seven decades). The diffusion coefficient D is given in units of 10^{-9} sm^{-2}.We give one example of 1) pure tumor, 2) pure fatty tissue, 3) fatty tumor, 4) fibrous mastopathy, and 5) liver tissue. We show the relaxation functions with both methods, i.e., at constant evolution time τ_2 and varying the wave vector (left graph) or varying the evolution time at fixed wave vector (right graph) side by side.

Relaxation functions

Pure tumor (Fig. 1)

Fatty tissue (Fig. 2)

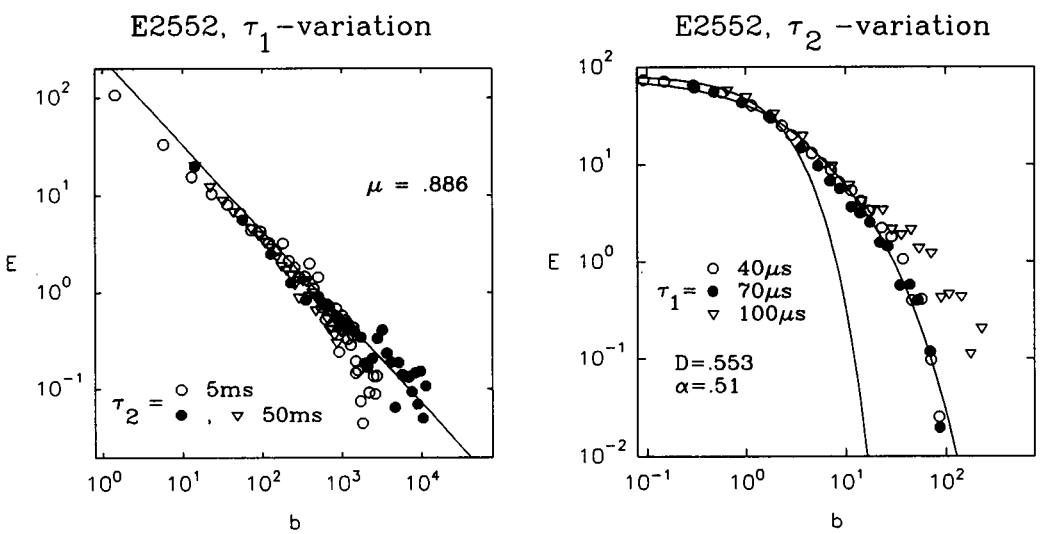

FIGURE 1 The relaxation function changes from Debye-like for short τ_2 to power law for long τ_2 (*left graph*). The evolution in time is described by a superposition of a Debye and KWW-function (*solid line*, $\chi^2 = 0.935$) with the same diffusion coefficient. For comparison, a single Debye function is shown with the same scaling (*dashed line*). This function is clearly insufficient for data description (*right graph*).

Fatty tumor (Fig. 3)

Fibrous mastopathy (Fig. 4)

Liver (Fig. 5)

Statistics

In general the μ-values, i.e., asymptotic slopes in left graphs of Figs. 1–5 increase with fatty content of the specimens. Thus the μ-values of cancerous tissues are in general lower than the μ-values of noncancerous as illustrated in Fig. 6.

To investigate the influence of fatty contributions we give the relaxation function of pure glandular tissue (liver, Fig. 5). In comparison to Fig. 2 the power law behavior is evident. Pure tumorous tissue (Fig. 1) is clearly comparable because of high epithelial content. The finding can be explained by the higher compartmentation (increased proliferation rate) of tumorous tissue in accordance with results previously obtained by quite different methods (Rose et al., 1993).

In cases of nonapplicability of the KWW function but compartmentation due to fatty content (see Figs. 2–4), this latter part correlated well with the histologically observed contribution. In contrast the KWW part showed no correlation to fatty content. Further, we observed the well-known negative correlation of T_1 with fatty content (data not shown).

Error estimates

In view of the rather large range covered by the echo amplitudes, considerations of data reproducibility, i.e., influence of noise and other possible error sources, are quite necessary. For this purpose the measurements with τ_2-variation were repeated under identical conditions as used to obtain the right graphs of Figs. 1–5 ~16 h later with one tumorous specimen as it was typically available. In Fig. 7 the arithmetic averages of the two series are depicted as points and the standard deviations as error bars, indicating a measure of reproducibility. In these experiments (see also right graphs of Figs. 1–5) one data point always represents an average over 20 accumulations—a rather low number compared to 600—used in the case of the longest τ_2-value in our second type of experiment. Nevertheless data scatter stays quite small over nearly two orders of magnitude in echo amplitude. The solid line represents the best fit obtained by a superposition of a Gaussian and KWW function accordingly (Eq. 5). The Chi-square value refers to the quality of the fit function to represent the indicated averages as data points.

A second error source originates from the necessary T_1-correction for the evolution interval; in general T_1 measurements in tissues are associated with an accidental error of ~10% (Bottomley et al., 1984). A more serious problem, however, is the appearance of tissue heterogeneity, leading to a superposition of exponential T_1-relaxation functions. This is most pronounced in the presence of fatty contributions, which show significantly lower T_1-values. This difference, however, is in general not sufficient to allow for a separation of relaxation contributions from fatty and nonfatty parts of the specimens. The calculation of T_1 is, therefore, performed by the spectrometer software with one average exponential function; and this value was used for T_1-correction. Therefore, in Fig. 7 we made no attempt to account for scatter in T_1-values from the above-mentioned 3–5 control measurements (see Materials).

DISCUSSION

We have used and pushed forward the rather new method of the supercon fringe field technique (Kimmich et al., 1991; Kimmich et al., 1994a) to investigate the diffusion process

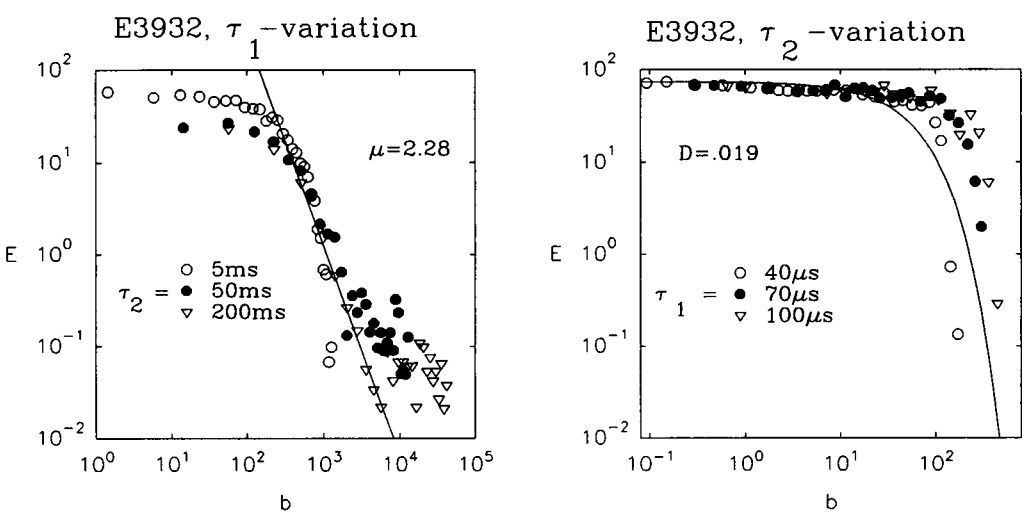

FIGURE 2 The relaxation function changes from Debye-like for short τ_2 to power law for long τ_2 (*left graph*). The limiting slope however is much steeper than in Fig. 1, indicating that the Debye function is adequate for the whole range of time scales, $\chi^2 = 0.446$.

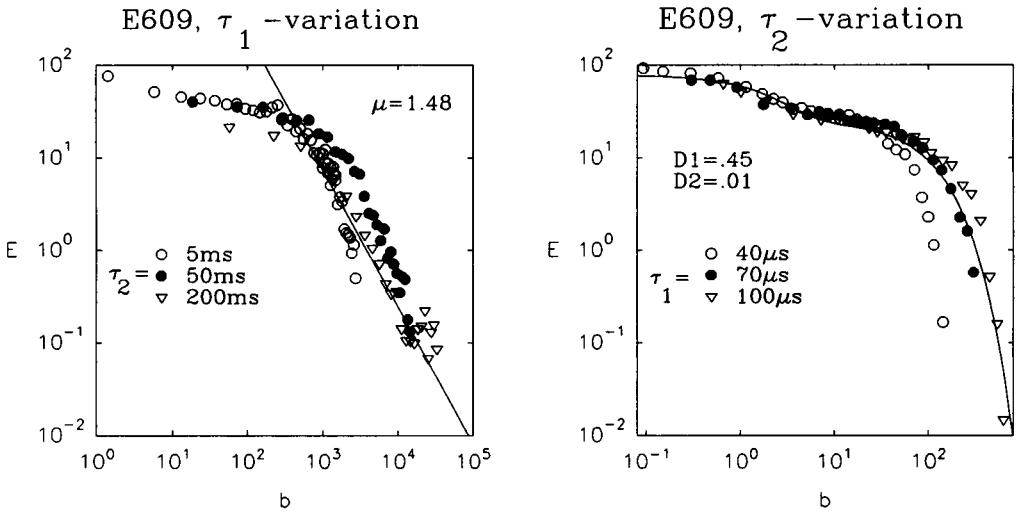

FIGURE 3 The relaxation function consists of a superposition of the properties described in Figs. 1 and 2 according to the relative contributions of tumorous and fatty tissue, which are comparable. The limiting slope is steeper than for the pure tumor and flatter than for fat (*left graph*). The evolution in time is described by a superposition of two Debye functions (Eq. 1) with diffusion coefficients of water and fat, $\chi^2 = 0.817$. The KWW part of the tumor component is overwhelmed by the contribution of fat cells (*right graph*).

in biological tissues. Because the method is sensitive to dynamic and structural properties of the specimen in the subcellular region via the diffusion coefficient and Fourier space description of probability density, the necessity arose to extend known theories from other topics (Shlesinger, 1985; Gosh and Chakrabarti, 1991; Nonnenmacher and Nonnenmacher, 1989; Nonnenmacher, 1994; Metzler et al., 1994; Montroll and Bendler, 1984; West and Shlesinger, 1989) to the new experimental conditions to get a conclusive description of the measurements. Our main goal was to check the possibilities of the technique in pathological tissue characterization. The two above-mentioned pure tumors (without fat, Fig. 1) produced rather similar relaxation functions. In general, however, the high heterogeneity of breast tissue does not allow such clear measurements (Figs. 2–4). This is in accordance with other nonimaging research (Eggleston et al., 1975; McSweeney et al., 1984; Bottomley et al., 1984) where the contribution of fatty parts of the specimens also presented problems. The breast is uniquely heterogeneous, being composed of fat, epthelial tissue, and fibrous supporting stroma in widely differing proportions. The marked individual variation in the composition of normal breast tissue, as well as numerous possible benign and malignant conditions, make it unlikely that a single relaxation function could adequately characterize the range of proton environments present (McSweeney et al., 1984). The results are at least not in contradiction to other criteria of histology and cell biology. The range of length (or inverse

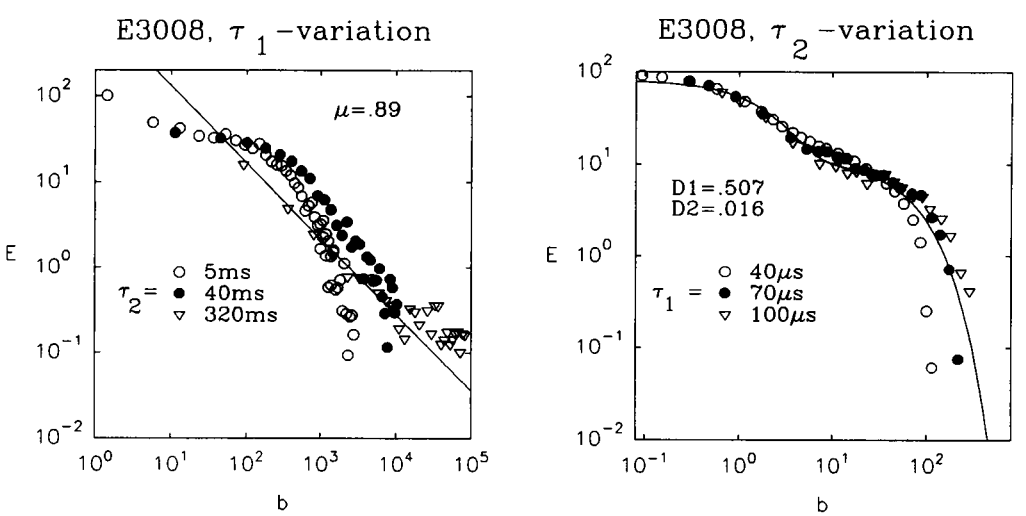

FIGURE 4 The relaxation function changes from Debye-like for short τ_2 to power law for long τ_2 (*left graph*). The evolution in time is described by a superposition of two Debye processes with diffusion coefficients of water and fat, $\chi^2 = 0.817$. The tissue consisted of comparable amounts of epithel, connective tissue, and fat.

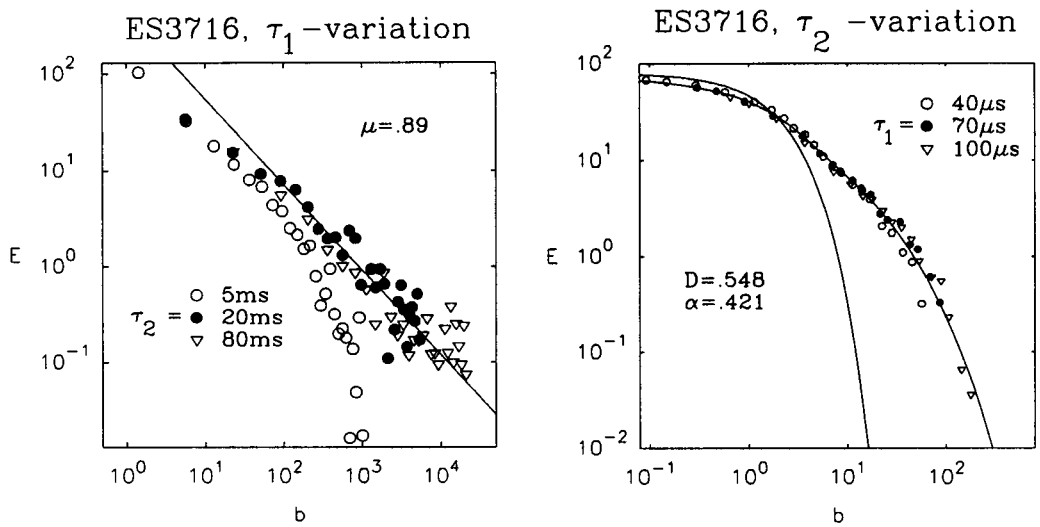

FIGURE 5 The relaxation function changes from Debye-like for short τ_2 to power law for long τ_2 (*left graph*). The evolution in time is described by a superposition of a Debye and KWW function with the same diffusion coefficient, $\chi^2 = 0.975$. For comparison a single Debye function with the same scaling is shown (*dashed line*). This function is clearly insufficient for data description (*right graph*).

wave vectors) and time scales accessible by the method cover specifically the cellular and subcellular regions; thus the method seems especially suited for these investigations. Clinical investigations are never based on NMR investigations alone, but also involve physiological and morphological aspects. The kind of method refers to rather different length scales, largely exceeding the cellular region in the case of imaging and so do methods and answers. At the moment the method seems far away from application in vivo, but offers a new method of basic research.

APPENDIX

The most successful NMR-method for measurement of diffusion is that of the stimulated echo, according to Tanner and Steijskal (1968), Callaghan (1991), and Kimmich et al. (1991). In short, the stimulated echo is produced by a sequence of three $\pi/2$ pulses, separated by two variable time spacings τ_1 and τ_2 as indicated in Fig. 8.

The fanning out of the isochromates during τ_1 is periodic in space with the wave vector

$$q = (2\pi)^{-1}\gamma_0 G\tau_1, \qquad \text{(A1)}$$

where γ_0 is the gyromagnetic ratio and G the field gradient. The spins get spatially encoded by their relative phase relations at the end of τ_1. During the second, generally longer evolution interval τ_2, the molecules diffuse in

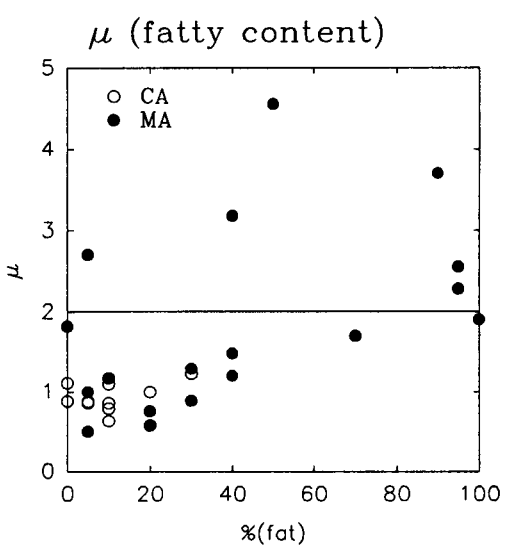

FIGURE 6 The asymptotic slope μ did not exceed the value 2 (*dashed line*) for 10 of 12 tumors with low fatty content. This is in contrast to fibrous diseases, reaching higher values irrespective of fatty content.

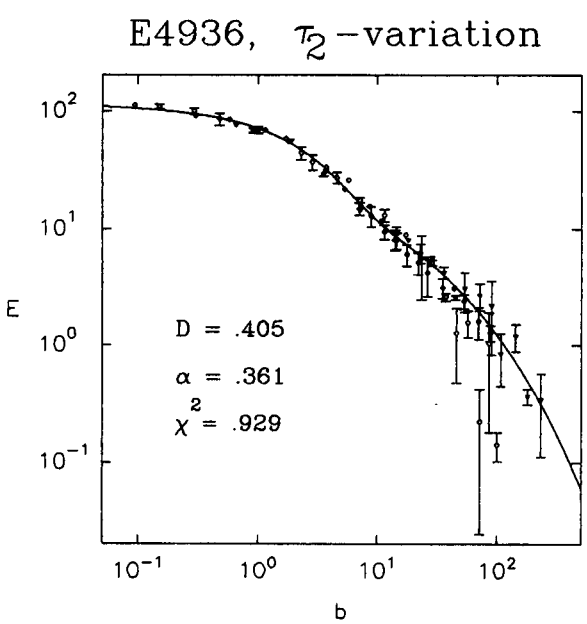

FIGURE 7 Illustration for data reproducibility; each point represents the arithmetic average of two measurements, the error bars indicate the standard deviation. To show the evolution in data scatter, the point size is smaller than in Figs. 1–5 (*right graphs*). The specimen contained about 50% epithel, 30% connective tissue, and 20% fat.

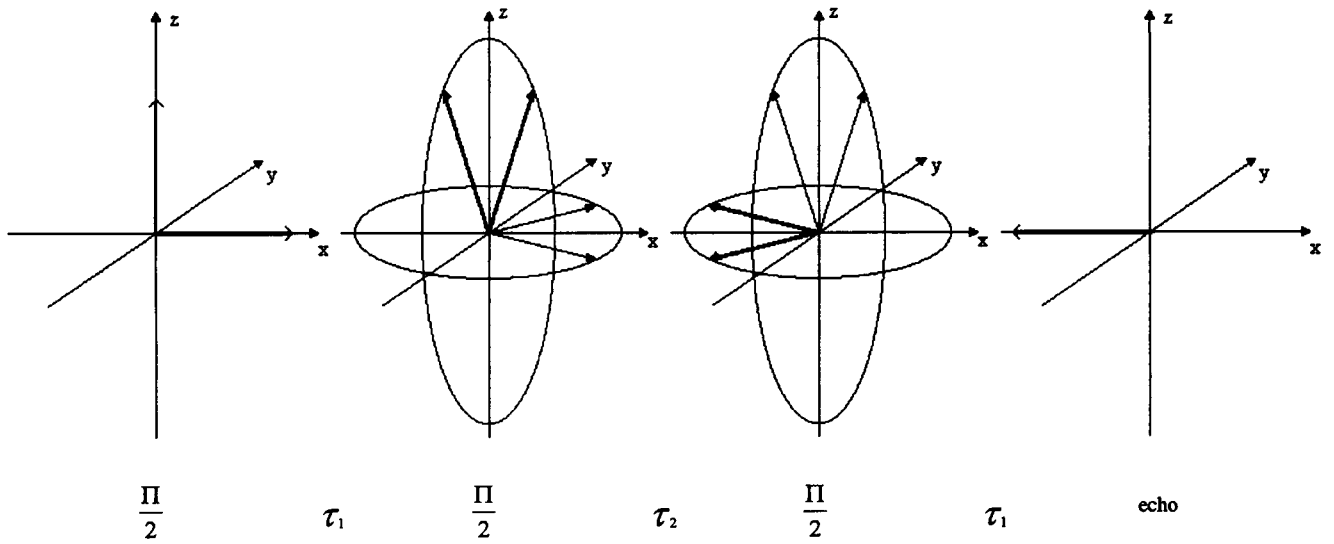

FIGURE 8 Principle of the stimulated echo method. The transversal magnetization, produced by the initial $\pi/2$ pulse, decays during τ_1 (preparation period) because of the spatially different Larmor frequencies in the gradient field. The second $\pi/2$ pulse rotates the spins from the x-y plane back to the z axis, conserving the phase relations among the spins. After the evolution interval τ_2, the third $\pi/2$ pulse rotates the magnetization again into the x-y plane, but the direction of the spins is inverted. The faster spins initially lag behind the slower ones and catch up with them to give the stimulated echo at time τ_1 after the third $\pi/2$ pulse (read period). Without additional dephasing during τ_2 because of diffusion, complete rephasing would occur. Thin (thick) arrows indicate the position of isochromats in a frame, which rotates at the mean Larmor frequency before (after) the corresponding pulses. An isochromat means the spins within an infinitesimally thin sheet within the field can be considered locally homogeneous, so all spins of the isochromat have the same local Larmor frequency. In general τ_1 and τ_2 are weighted by the transversal (T_2) and longitudinal (T_1) relaxation times of dipolar interaction, respectively, affording a corresponding correction. In biologic tissue T_2 is always about 40 ms ("free" bulk water) and 5 ms (hydration water), much larger than the longest τ_1-values ($\sim$1 ms) and can therefore be neglected. However τ_2 reaches the order of T_1; this correction is quite necessary and routinely applied. The condition $\tau_1 \ll \tau_2$ (narrow pulse approximation) assumes that negligible diffusion occurs during τ_1 (compared to τ_2), leading to an effective separation of time scales and is always given because of the high gradient. The primary echo forms at time τ_1 after the second $\pi/2$ pulse in close resemblance to the Hahn echo (not shown).

space, each suffering an additional net shift in phase. The third pulse leads to a partial refocusing of the isochromates at τ_1 after the third pulse. The amplitude of this ensemble-averaged residual transversal magnetization is determined by the net phase shift of all nuclear spins during the evolution interval τ_2. The shift of an isochromate is caused by the accumulation of phase shifts due to random migration to places of different field strengths of Larmor frequencies during this time interval. This ensemble average, in which each phase term is weighted by the probability for a spin to begin at r and move to r'in time τ_2, is given by Callaghan (1991)

$$E = \int_{-\infty}^{\infty} \rho(r) \int_{-\infty}^{\infty} P(r|r', \tau_2) \exp[i\gamma_o \tau_1 G(r' - r)] dr' dr \quad (A2)$$

In this general expression $\rho(r)$ is the probability of finding a molecule at initial time at place r, giving rise to the nomenclature "a priori probability density" and is representative of the static structure or form of the investigated object (here: the cell structure). $P(r|r',\tau_2)$ is the conditional probability for a molecule, initially at its starting point r, to be found at r'after the time interval τ_2. This function for normal diffusion is simply a spreading Gaussian bell shaped curve. As it turns out, it is especially the bell shaped form and its evolution in time that are subject to essential modification. Assuming homogeneity of the sample, meaning simply that variations in structure or $\rho(r)$ occur on a much smaller scale than the resolution or q^{-1}, it is possible to define an ensemble-averaged propagator P_s. This quantity presumes that the mean spread of the probability function is independent of the starting points r or the structure. With this assumption, the phase shifts in the integrand of the above expression (Eq. A2) depend only on the net displacement $R = r'$-r. Thus Eq. A2 gets the form

$$E = \int_{-\infty}^{\infty} P_s(R, \tau_2) \exp(i2\pi qR) dR. \quad (A3)$$

The signal amplitude corresponds to the Fourier transform of mean conditional probability density.

As mentioned above, the case of normal standard diffusion is described by a spreading Gaussian function:

$$P_s(R, \tau_2) = (4\pi D\tau_2)^{-(1/2)} \exp(-R^2/4D\tau_2) \quad (A4)$$

(in one dimension). The insertion in Eq. A3 gives the usual Debye expression

$$E = \exp(-4\pi^2 q^2 \tau_2 D) = :\exp(-Db) \quad (A5)$$

One notices, that the quantity $b = 4\pi^2 q^2 \tau_2$ is already a space-averaged quantity, implying the same dynamic behavior in all parts of the sample; this assumption is clearly given in pure fluids, but quite unrealistic in systems of high heterogeneity. A special complication in our theory is that we are dealing simultaneously with dynamic and structural parameters according to the general form (Eq. A2). In the presence of structure, diffusion is no longer of the Debye form (Eq. A5) but becomes anomalous.

The ensemble-averaged mean square displacement in the case of anomalous diffusion (d_w>2 is the anomalous diffusion exponent (Metzler et al., 1994), special case $d_w = 2$ corresponds to averaging with respect to a

Gaussian profile, Eq. A4) is given by

$$\langle R^2 \rangle \sim \tau_2^{2/d} w. \tag{A6}$$

For reason of integer dimensionality of the diffusion coefficient we chose to write the relaxation function of a stretched exponential (Shlesinger, 1985; Gosh and Chakrabarti, 1991) in the form

$$E = \exp[-(Db)^{\alpha}]. \tag{A7}$$

This holds at least in the small and intermediate q region. By increasing q, deviations from this dependence appear. The nature of these deviations becomes more evident in the second series of measurements, keeping τ_2 large and fixed, while stepping the wave vector. The observed relaxation function in this case is a Fourier description of the probability density according to Eq. A2. At short τ_2 it is often difficult to give a reliable formula for an appropriate description; at the longest τ_2-values and/or largest q values, however, the most suitable form for data description is the "long tail" (Nonnnenmacher and Nonnenmacher, 1989; Nonnenmacher 1994) with the asymptotic inverse power law representation

$$E \sim (q^2)^{-\mu} \tag{A8}$$

for large times τ_2. This form is also given by Fourier transforming the solution of the diffusion equation on a fractal structure with dimension 2 μ (Metzler et al., 1994).

To understand the empirical inverse power law ansatz (Eq. A8) within the context of Lévy statistics we go back to Eq. A3, choosing for $P_s(R, \tau_2)$ a generalization of the Gaussian probability profile (Eq. A4), i.e., we take a KWW probability density profile

$$P_s(R, \tau_2) = C_0 \exp[-(R/\sigma)^{\beta}], \quad \sigma = (4D\tau_2)^{1/d} w \tag{A9}$$

C_0 is the normalization constant), which leads (when inserted into (A3)) to the following representation (Montroll and Bendler, 1984; Glöckle and Nonnenmacher, 1993) for the Lévy distribution function:

$$E(q) = (\beta/\Gamma(1/\beta)) \sum_{n=1}^{\infty} (-1)^{n+1}[\Gamma(1 + \beta n)/n!] \cdot (2\pi q\sigma)^{-(1+\beta n)} \sin(\pi\beta n/2) \tag{A10}$$

For

$$2\pi q\sigma \gg 1, \tag{A11}$$

the result (Eq. A10) approaches the asymptotic formula

$$E(q) \approx (\beta/\Gamma(1/\beta))\Gamma(1 + \beta)\sin(\pi\beta/2) \cdot (2\pi q\sigma)^{-(1+\beta)} \sim q^{-(1+\beta)} \tag{A12}$$

Comparing this result with Eq. A8, we find for sufficiently large σ the index law

$$2\mu = 1 + \beta, \tag{A13}$$

which relates the index β of Eq. A9 via Eqs. A12 and A13 to the inverse power law index μ of Eq. A8. Our experiments carried out at constant, large τ_2 values satisfy the condition (Eq. A11) for the wave vector region q under consideration, and consequently we expect that the data should follow the asymptotic inverse power law (Eq. A12). Indeed, that is precisely what we observe for this sort of experiment (see left graphs of Figs. 1–5). Thus, to our knowledge, we have demonstrated for the first time direct evidence for long tail Levy statistics that forms the basic concept for our interpretation of NMR measurements of slow diffusion dynamics in fresh tissue specimens.

Dr. T. F. Nonnenmacher was supported by grant SFB 239 from Deutsche Forschungsgemeinschaft.

REFERENCES

Bottomley, P. A., T. H. Foster, R. E. Aragersinger, and L. M. Pfeifer. 1984. A review of normal tissue hydrogen NMR relaxation times and relaxation mechanisms from 1–100 MHz: dependence on tissue type, NMR frequency, temperature, species, excision, and age. *Med. Phys.* 11: 425–448.

Callaghan, P. T. 1991. Principles of NMR Microscopy. Oxford University Press, New York.

Cheng, K. H. 1993. Quantitation of non-Einstein diffusion behaviour of water in biological tissues by proton MR diffusion imaging: synthetic image calculations. *Magn. Reson. Imaging.* 11:569–583.

Drost-Hansen, W., and J. Clegg. 1976. Cell-Associated Water. Academic Press, Inc, London.

Eggleston, J. C., L. A. Saryan, and D. P. Hollis. 1975. Nuclear magnetic resonance investigations of human neoplastic and abnormal nonneoplastic tissues. *Cancer Res.* 15:1326–1332.

Fujara, F., E. Ilyina, H. Nienstaedt, H. Sillescu, R. Spohr, and C. Trautmann. 1994. Anisotropic diffusion in etched particle tracks studied by field gradient NMR. *Magn. Reson. Imaging.* 12:245–246.

Glöckle, W. G., and T. F. Nonnenmacher. 1993. Fox function representation of non-Debye relaxation processes. *J. Stat. Phys.* 71:741–757.

Glöckle, W. G., and T. F. Nonnenmacher. 1995. A fractional calculus approach to self-similar protein dynamics. *Biophys. J.* 68:46–53.

Gosh, M., and B. K. Chakrabarti. 1991. Relaxation in disordered systems. *Indian J. Phys.* 65A:1–24.

Hazlewood, C. F., D. C. Chang, B. L. Nichols, and D. E. Woessner. 1974. Nuclear magnetic resonance. Transversal relaxation times of water protons in skeletal muscle. *Biophys. J.* 14:583–606.

Hazlewood, C. F., H. E. Rorschach, and C. Lin. 1991. Diffusion of water in tissues and MRI. *Magn. Reson. Med.* 19:214–216.

Ishida, N., H. Ogawa, and H. Kano. 1995. Diffusion of cell-associated water in ripening barley seeds. *Magn. Reson. Imaging.* 13:745–751.

Kimmich, R., and E. Fischer. 1994a. One- and two-dimensional pulse sequences for diffusion experiments in the fringe field of superconducting magnets. *J. Magn. Reson.* A106:229–235.

Kimmich, R., S. Stapf, P. T. Callaghan, and A. Coy. 1994b. Microstructure of porous media probed by NMR techniques in sub-micrometer length scales. *Magn. Reson. Imaging.* 12:339–343.

Kimmich, R., W. Unrath, G. Schnur, and E. Rommel. 1991. NMR measurement of small self- diffusion coefficients in the fringe field of superconducting magnets. *J. Magn. Reson.* 91:136–140.

Le Bihan, D., E. Breton, D. Lallemand, P. Grenier, E. Cabnis, and M. Laval-Jeantet. 1986. MR imaging of intravoxel incoherent motions: application to diffusion and perfusion in neurologic disorders. *Radiology.* 161:401–407.

McSweeney, M. B., W. C. Small, V. Cerney, W. Sewell, R. W. Powell, and J. H. Goldstein. 1984. Magnetic resonance imaging in the diagnosis of breast disease: Use of transversal relaxation times. *Radiology.* 153: 741–744.

Metzler, R., W. G. Glöckle, and T. F. Nonnenmacher. 1994. Fractional model equation for anomalous diffusion. *Physica A.* 211:13–24.

Montroll, E. W., and J. T. Bendler. 1984. On Lévy (or stable) distributions and the Williams-Watts model of dielectric relaxation. *J. Stat. Phys.* 34:129–162.

Nonnenmacher, T. F. 1994. Fractals in Biology and Medicine. Birkhäuser Verlag, Basel, Germany.

Nonnenmacher, T. F., and D. J. F. Nonnenmacher. 1989. A fractal scaling law for protein gating kinetics. *Phys. Lett.* A140:323–326.

Norris, D. G., T. Niendorf, M. Hoehn-Berlage, K. Kohne, E. J. Schneider, P. Hainz, M. Hropot, and D. Leibfritz. 1994. Incidence of apparent restricted diffusion in three different models of cerebral infarction. *Magn. Reson. Imaging.* 12:1175–1182.

Rose, Ch., T. Mattfeldt, M. Köpf, and O. Haferkamp. 1993. ^{31}Phosphor-NMR-Spektroskopie an Mastopathien und duktal-invasiven Mammakarzinomen. *Verh. Dtsch. Ges. Pathol.* 77:432.

Shlesinger, M. F. 1985. Derivation of the Kohlrausch-Williams/Watts decay law from activation-energy dispersion. *Macromolecules.* 18: 591–592.

Tanner, J. E., and E. O. Steijskal. 1968. Restricted self-diffusion of protons in colloidal systems by the pulsed-gradient, spin-echo method. *J. Chem. Phys.* 49:1768–1777.

Taylor, D. G., R. Inamdar, and M-C Bushell. 1988. NMR imaging in theory and in practice. *Phys. Med. Biol.* 33:635–670.

West, B. J., and M. F. Shlesinger. 1989. On the ubiquity of 1/f noise. *Int. J. Mod. Phys.* B3:795–819.

West, B. J., and W. Deering. 1994. Fractal physiology for physicists: Lévy statistics. *Phys. Rep.* 246:1–100.

Zumofen, G., A. Blumen, J. Klafter, and M. F. Shlesinger. 1989. Lévy walks for turbulence: a numerical study. *J. Stat. Phys.* 54:1519–1528.